Turkish Journal of Electrical Engineering & Computer Sciences

http://journals.tubitak.gov.tr/elektrik/

Research Article

Turk J Elec Eng & Comp Sci
(2019) 27: 2444 – 2455

doi:10.3906/elk-1901-233

All-polymer ultrasonic transducer design for an intravascular ultrasonography application

Dooyoung HAH*
Department of Electrical & Electronics Engineering, Faculty of Engineering, Abdullah Gül University, Kayseri, Turkey

Received: 31.01.2019 • **Accepted/Published Online:** 24.05.2019 • **Final Version:** 26.07.2019

Abstract: Intravascular ultrasonography (IVUS), a medical imaging modality, is used to obtain cross-sectional views of blood vessels from inside. In IVUS, transducers are brought to the proximity of the imaging targets so that high-resolution images can be obtained at high frequency without much concern of signal attenuation. To eliminate mechanical rotation rendered in conventional IVUS, it is proposed to manufacture a transducer array on a flexible substrate and wrap it around a cylindrical frame. The transducer of consideration is a capacitive micromachined ultrasonic transducer (CMUT). The whole device needs to be made out of polymers to be able to endure a high degree of bending (radius: 1 mm). Bending of the devices leads to considerable changes in the device characteristics, including resonant frequency and pull-in voltage due to geometrical dimension changes and stress induced. The main purpose of this work is to understand the effect of bending on the device characteristics by means of finite element analysis. Another objective of the work is to understand the relationships between such an effect and the device geometries. It is learned that the bending-induced stress depends strongly on anchor width, membrane thickness, and substrate thickness. It is also learned that resonant frequency and pull-in voltage become lower in most cases because of using a flexible substrate in comparison to those of the device on a rigid substrate. Bending-induced stress increases the spring constant and hence increases resonant frequency and pull-in voltage, although this effect is relatively weaker. For most of the device geometries, pull-in voltage is too high for the polymer material to endure. This is the main drawback of the all-polymer CMUT. In order to meet the design goal of 20 MHz resonant frequency, the membrane radius has to be smaller than 7.7 μm for a thickness of 3 μm.

Key words: Polymer microelectromechanical systems, ultrasonic transducer, flexible substrate, intravascular ultrasonography

1. Introduction

Ultrasonic imaging is a routinely used tool for medical diagnosis and therapeutic interventions. As one of its special branches, intravascular ultrasonography (IVUS) brings ultrasonic transducers to the close proximity of the imaging targets, i.e. blood vessels, so that high frequency (20–40 MHz) acoustic waves can be used for better resolution (typically, lateral: 0.2–0.25 mm, axial: 0.08 mm) without much concern of signal attenuation [1–5]. In conventional side-firing IVUS, to obtain radial images of a blood vessel from inside, mechanical rotation of either one transducer or a linear array of transducers has been rendered through external control. In order to carry out the imaging procedure in a less complicated way and to be able to reach deeper regions, it is desirable to eliminate the need for such mechanical rotation. One way to achieve such a goal is to manufacture

*Correspondence: dooyoung.hah@agu.edu.tr

the transducer array either on a flexible or on a foldable substrate, and to wrap it around a cylindrical frame (diameter: 1–2 mm); a conceptual illustration is presented in Figure 1 [6–13]. Bending of ultrasonic transducers around such a small radius can alter their characteristics, such as mechanical resonant frequency, pull-in voltage, and so on. Moreover, in some cases, such a wrapping can even cause substantial deformation and stress, leading to structural and functional failure in the transducers. In this work, finite element analysis (FEA) is used to study those effects, and a design guideline is presented based on the findings.

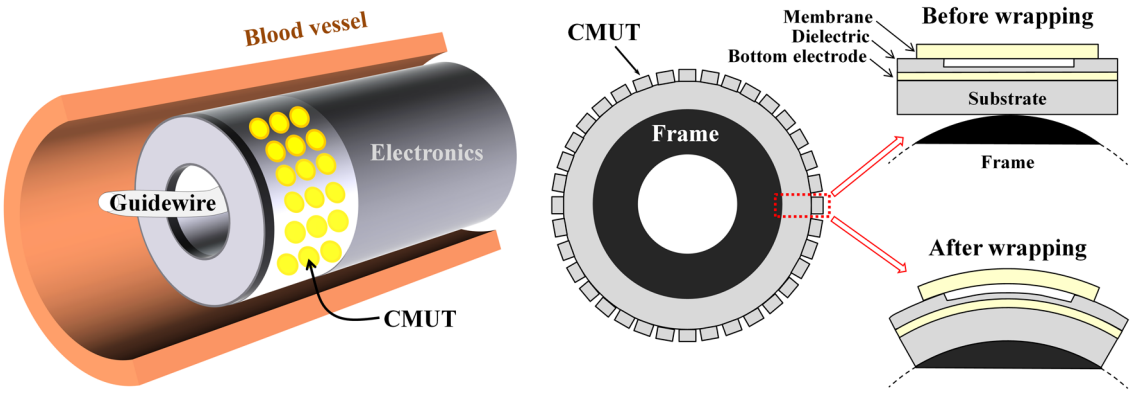

Figure 1. A proposed ultrasonic probe with radial CMUTs on a flexible substrate for IVUS. Left: A probe inside a blood vessel. Right: A cross-section view of a probe.

There are two major transduction mechanisms that have been used mainly in miniaturized ultrasonic probes: capacitive and piezoelectric. The device utilizing the former mechanism is called a capacitive micromachined ultrasonic transducer (CMUT) [14–16]. The one with the latter is called a piezoelectric micromachined ultrasonic transducer (PMUT) [17, 18]. In general, CMUT devices show better impedance matching in air/fluid coupling than PMUTs, while PMUT devices are relatively easier to fabricate than CMUTs. In this work, CMUT devices are considered for the study. Figure 1 also presents a cross-section view of a proposed CMUT device. It consists of a conducting membrane, a dielectric layer, and a bottom electrode on a flexible substrate. The dielectric layer is recessed to create an air gap so as to give clearance for the membrane to deform. The role of the dielectric layer underneath the membrane is to prevent direct contact between the membrane and the bottom electrode in case the membrane collapses due to a pull-in phenomenon. The operation principle of the CMUT is relatively straightforward. An AC voltage is applied between the membrane and the bottom electrode to make the membrane vibrate, which produces an ultrasound wave. When the reflected acoustic signal arrives at the membrane to induce vibration, it is detected through reading the resulted capacitance change. Typically, a DC voltage is applied as a bias to bring the membrane closer to the bottom electrode. It is well documented that biasing the device near the pull-in voltage increases the coupling from electrical energy to mechanical energy [15]. Typically, the transducers are biased at 80%–90% of the pull-in voltage. There is an adverse effect in biasing as well. Due to the electrical spring softening effect, the mechanical resonant frequency of the membrane is reduced as the dc bias is applied [19].

The organization of the paper is as follows. Section 2 will describe the materials and methods of the study. The results will be presented in Section 3 along with discussions.

2. Materials and methods

2.1. Material selection

Previously, the author reported the design of polysilicon-based CMUTs on a flexible substrate [13]. The effect of bending around a cylindrical frame on the device characteristics was studied. A polysilicon-based material set was selected for its good material properties and well-established fabrication processes. The main drawback of the polysilicon-based CMUTs was stress generated while wrapping around a frame, which is large enough to separate the membranes from the flexible substrate. One can reduce the stress by modifying the device geometries, i.e. thin and large membranes. However, this lowers the resonant frequency so that the design goal (i.e. 20 MHz) cannot be met. Therefore, it is necessary to search for an alternative material set.

Among others, two aspects are more imperative for the material selection: longitudinal wave velocity and maximum strain before yielding. As the following equation shows, longitudinal wave velocity is a material property, to which mechanical resonant frequency is directly proportional:

$$\text{Longitudinal wave velocity} = \sqrt{\frac{\text{Young's modulus}}{\text{density}}} \propto \sqrt{\frac{\text{spring constant}}{\text{mass}}} \propto \text{resonant frequency.} \tag{1}$$

Maximum strain before yielding is a good indication to understand material flexibility, which can be calculated by dividing yield strength by Young's modulus. Figure 2 presents the values of these two parameters for a number of materials that are frequently used in microelectromechanical systems (MEMS) technologies. Silicon-based materials are found at the top-left corner of the graph, which means high resonant frequency and low flexibility. Polymer materials are found at the bottom-right corner, and metals are in between these two groups. The most desirable corner in the graph is the top-right (high resonant frequency and more flexibility) where no material is found. Therefore, polymers are selected for the proposed device because flexibility is an essential necessity to realize the device.

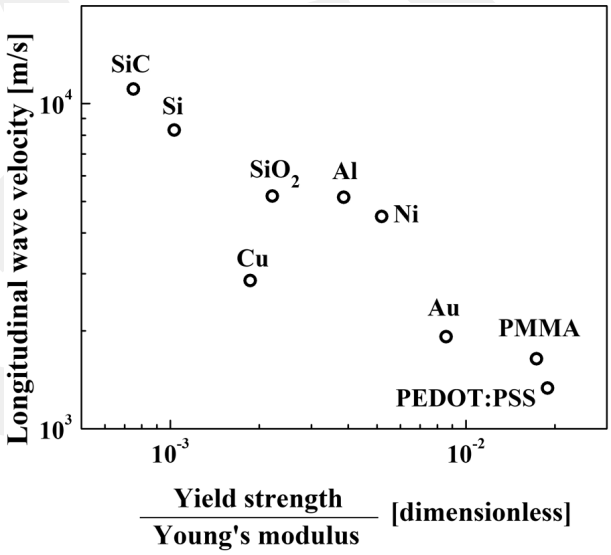

Figure 2. Longitudinal wave velocity and maximum strain before yielding for selected materials used in MEMS.

Electrical properties are also important for the membrane and the bottom electrode so that voltage can be effectively applied to them. Poly(3,4-ethylenedioxythiophene) polystyrene sulfonate or PEDOT:PSS (Young's

modulus: 1.6–2.0 GPa, tensile strength: 33–52 MPa, electrical conductivity: tens to thousands S/cm), one of the most widely used conductive polymers, is considered for this purpose. For the dielectric layer and the substrate, poly(methyl methacrylate) or PMMA (Young's modulus: 2.2–3.1 GPa, tensile strength: 52–71 MPa, dielectric constant: 2.6 @ 1 MHz) is selected in this study.

2.2. Design considerations

The main design target is 20 MHz of resonant frequency in consideration of the state-of-the-art IVUS probes and previous works in the literature. Ultrasound at 20 MHz has a wavelength of 77 μm in the tissues of the human body. The devices will be designed to be wrapped around a cylindrical frame with a diameter of 2 mm. Another design constraint is the number of elements in one array (typically, 32 to 128 elements in one row), which determines the number of azimuthal pixels in one cross-section view in the obtained image. To accommodate 64 elements in one row around a 2-mm-diameter frame, for example, the diameter of the transducer has to be smaller than 68.7 μm, assuming 70% fill factor. In regards to the number of elements in an array, a number of cables to drive and to read out the transducers have to be considered as well from the packaging point of view due to the small diameter of the catheter that delivers the probe to the inner part of the body. Integration of multiplexers near the probe has been used in some works in order to reduce the number of cables needed in the catheter [10]. The voltage used for the operation of the transducers cannot be too high for safety reasons since they are to be used inside the human body, even considering that the cables are electrically insulated. Another issue is with the low dielectric strengths of typical polymer materials.

2.3. Method: finite element analysis study

In order to understand the effects of substrate-bending on the device characteristics, and also to comprehend its relations to the device geometries, three-dimensional finite element analysis (FEA) was carried out by using COMSOL Multiphysics (version 5.2). Bending of the substrate was simulated by taking a fraction of the substrate—one-quarter of a transducer is considered in order to reduce computation time, taking advantage of the symmetry—and fixing one edge of the bottom surface and then applying a shear load to the side face that does not coincide with the fixed edge. For each device geometry, a proper magnitude of the shear load was found, which results in a deformation of the substrate equivalent to bending around a radius of 1 mm. Although the displacement profile is not exactly circular, this approximation is deemed acceptable since the magnitude of displacement is considerably small, i.e. about 450 nm of displacement in comparison to a bending radius of 1 mm, more than a thousand times of difference. Symmetrical boundary conditions were used in the lateral directions. Mechanical modal analysis was used to find resonant frequencies (eigenmodes). Pull-in (membrane collapse) voltages were found by coupling electrostatic and structural domain analyses. Seven different geometrical features were selected as the design parameters, as illustrated in Figure 3 and summarized in the Table. The Table also includes the nominal value (a default value when not varying) for each parameter. Simulation results will be presented in the following section.

3. Results and discussions

3.1. Deformation by bending

As described earlier, wrapping around a cylindrical frame was simulated by applying a shear load to the side surface in the negative z direction. For example, a shear load of 2 MPa was applied in the case of the nominal

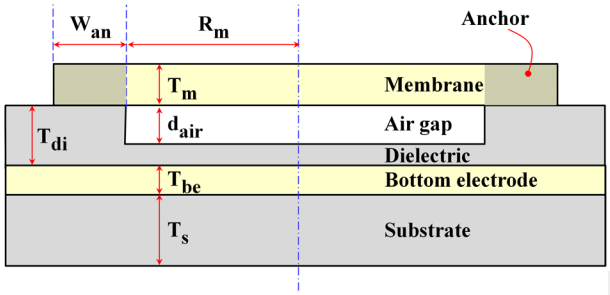

Figure 3. Geometrical design parameters of the CMUT device on a flexible substrate (cross-section view).

Table 1. Device geometries considered for design as well as the nominal values.

Description	Symbol	Nominal value μm
Membrane radius	R_m	10
Membrane thickness	T_m	3
Anchor width	W_{an}	18
Dielectric layer thickness	T_{di}	0.25
Bottom electrode thickness	T_{be}	1
Substrate thickness	T_s	10
Air gap thickness	d_{air}	0.15

device geometries. Figure 4a shows the calculated displacements in the z direction after bending, and Figure 4b shows the displacements of the membrane and the dielectric along the centers in both directions (x and y). Figure 4c shows an exemplifying image of meshing used for the structural mechanical simulation. A physics-controlled mesh creation option (available in COMSOL Multiphysics, tetrahedral type) was used. The lateral dimensions of the simulation domain are set to be 30 μm $\times$ 30 μm. It can be learned that the displacement occurs mostly along the x direction while that along the y direction is much smaller, which is as expected since the bending is applied in the y direction. It can also be seen that there is a displacement of about 20 nm along the center (y) of the dielectric layer. This is understood as a global displacement of the top surface of the dielectric due to shrinkage of the flexible substrate in z direction in response to its extension in the x direction when the substrate is bent. At the center point, the displacement of the membrane is 21 nm more than that of the dielectric, which means that the air gap is reduced due to bending by that amount. Figure 4d presents the air gap along the centers after bending. It is noted that the air gap thickness at the edge of the membrane is slightly less than the one before bending (150 nm). This is again due to shrinkage of the material in the z direction by bending. The change in the air gap affects the pull-in voltage, which will be discussed in Section 3.4.

3.2. Stress

Distribution of von Mises stress (Figure 5) was calculated for the device, which is induced by substrate bending. In order to prevent plastic deformation of materials, the highest stress induced should be below the yield strength of the corresponding material. As expected, the highest stress occurs at the interface between two different materials, especially at the geometrical discontinuities such as anchor edges as shown from the magnified parts in the figure. High stress concentration at the bottom of the substrate is merely due to an imposed boundary

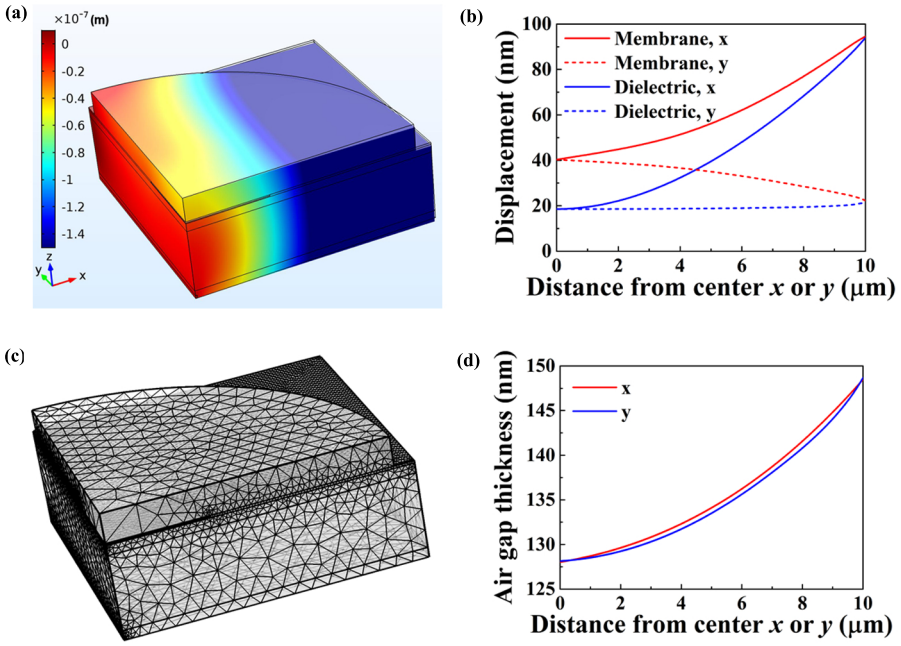

Figure 4. (a) Calculated displacement in z direction by bending around a 2-mm-diameter frame. A quarter of a single CMUT device is considered in order to shorten the computation time, by using symmetric boundary conditions applied on the central side surfaces. Nominal values (Table) are used for the device geometries. (b) Displacement (absolute value, in z direction) along the centers of the membrane and the dielectric. (c) Image of meshing used in the structural mechanical simulation. (d) Air gap thickness along the centers of the membrane after bending. Bending is performed in y direction.

condition, which is not imperative in the actual situation.

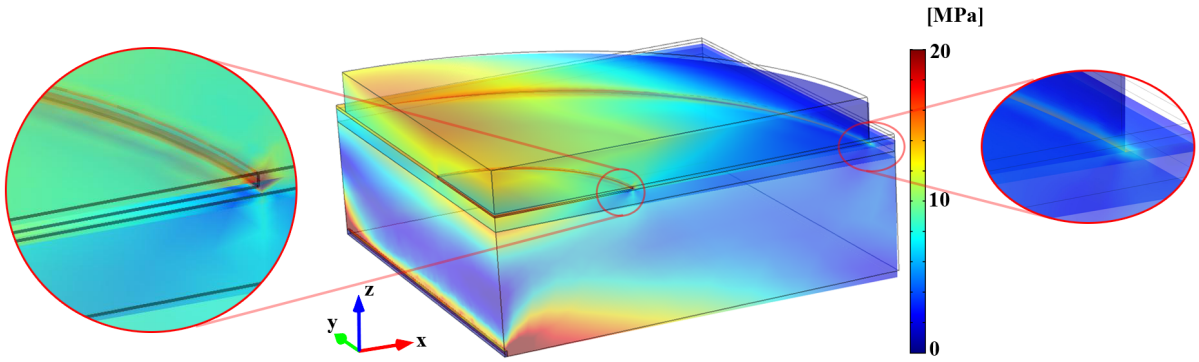

Figure 5. Stress distribution of a device after bending around a 2-mm-diameter frame, with magnified views around anchor edges. Bending is performed in the y direction. One-quarter of a CMUT is considered for simulation.

Figure 6 presents the relationships between the device geometries and the highest stress within each of the membrane, bottom electrode, and dielectric layers. It turns out that the anchor width (W_{an}), the membrane thickness (T_m), and the substrate thickness (T_s) affect the stress most significantly. Other parameters have moderate to low effects on the stress. For a narrow anchor width (< 8.1 μm), a thick membrane (> 4.7 μm), or a thick substrate (> 28.0 μm), the maximum stress goes beyond the yield strength of PMMA. The trend is

the same for the stress in the membrane (PEDOT:PSS), while the effect results in a more serious outcome than it does to the dielectric layer, i.e. the maximum stress becomes more than the yield strength when $W_{an} < 15.5$ μm, $T_m > 3.6$ μm, and $T_s > 12.0$ μm. These latter constraints, therefore, become the design guideline. In all cases, the induced stress is lower in the bottom electrode compared to the membrane because there is no boundary condition discontinuity in the former.

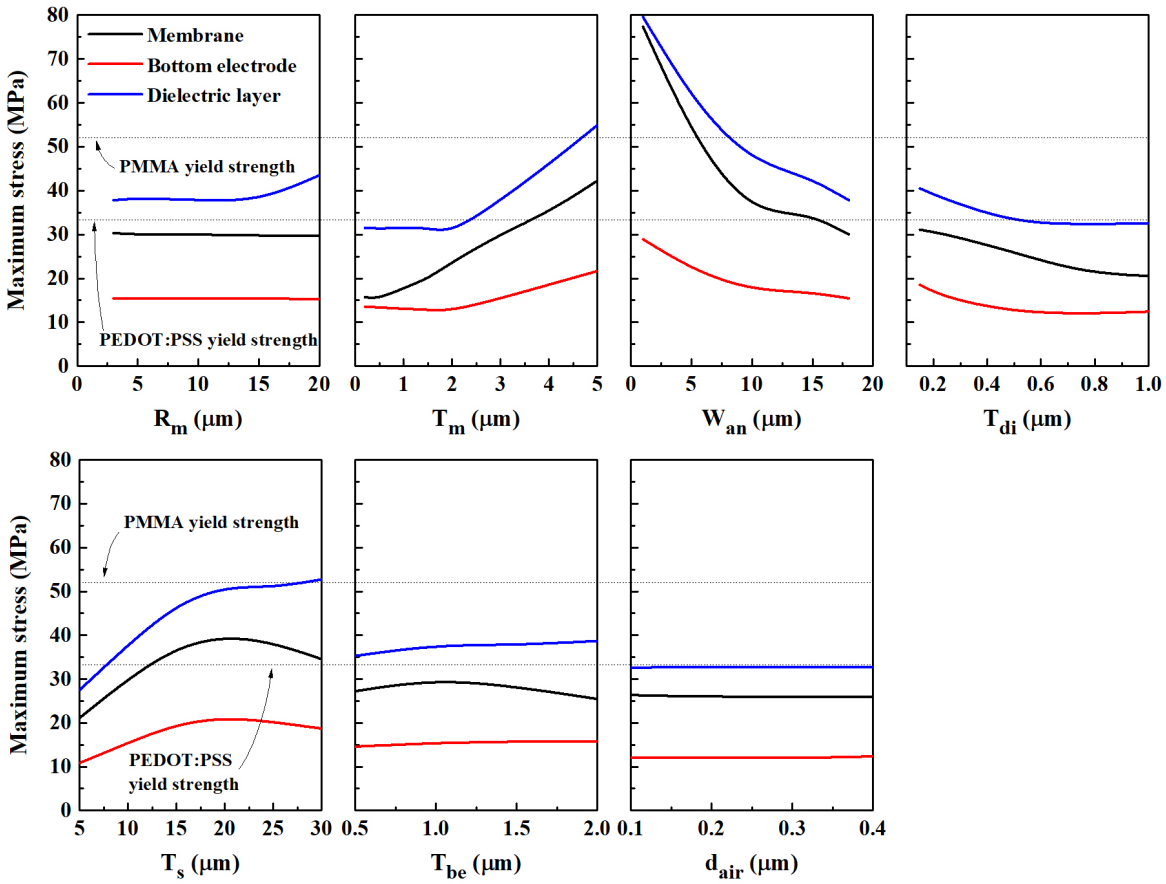

Figure 6. Maximum stress in membrane (black, PEDOT:PSS), bottom electrode (red, PEDOT:PSS), and dielectric layers (blue, PMMA) after bending around a 2-mm-diameter frame. Bending is performed in the y direction. Nonvarying geometries are set to the nominal values (Table), except for the following cases: (1) for varying R_m, W_{an} is changed as well to keep $R_m + W_{an}$ constant as 28 μm; (2) for varying T_{di}, d_{air} is set to be T_{di} - 0.1 μm; (3) for varying d_{air}, T_{di} is 0.5 μm. Auxiliary lines indicate yield strengths (the lowest in the range reported) of PMMA and PEDOT:PSS, respectively.

3.3. Resonant frequency

The effects of device geometries, flexibleness of the substrate, and bending of the substrate to the resonant frequency of the transducer membrane were studied by using FEA and are plotted in Figures 7a and 7b. When a membrane is fixed to a rigid substrate, it typically has one resonant frequency, which is associated with a fundamental mode profile. However, when it is sitting on a flexible substrate, more than one resonant mode is found, which have fundamental mode profiles in the membrane because the whole structure becomes a coupled oscillator, and the fundamental mode of the membrane can be coupled to a number of modes in the substrate. Figure 7c shows the deformation profiles of the device (nominal geometry in Table) for the resonant modes

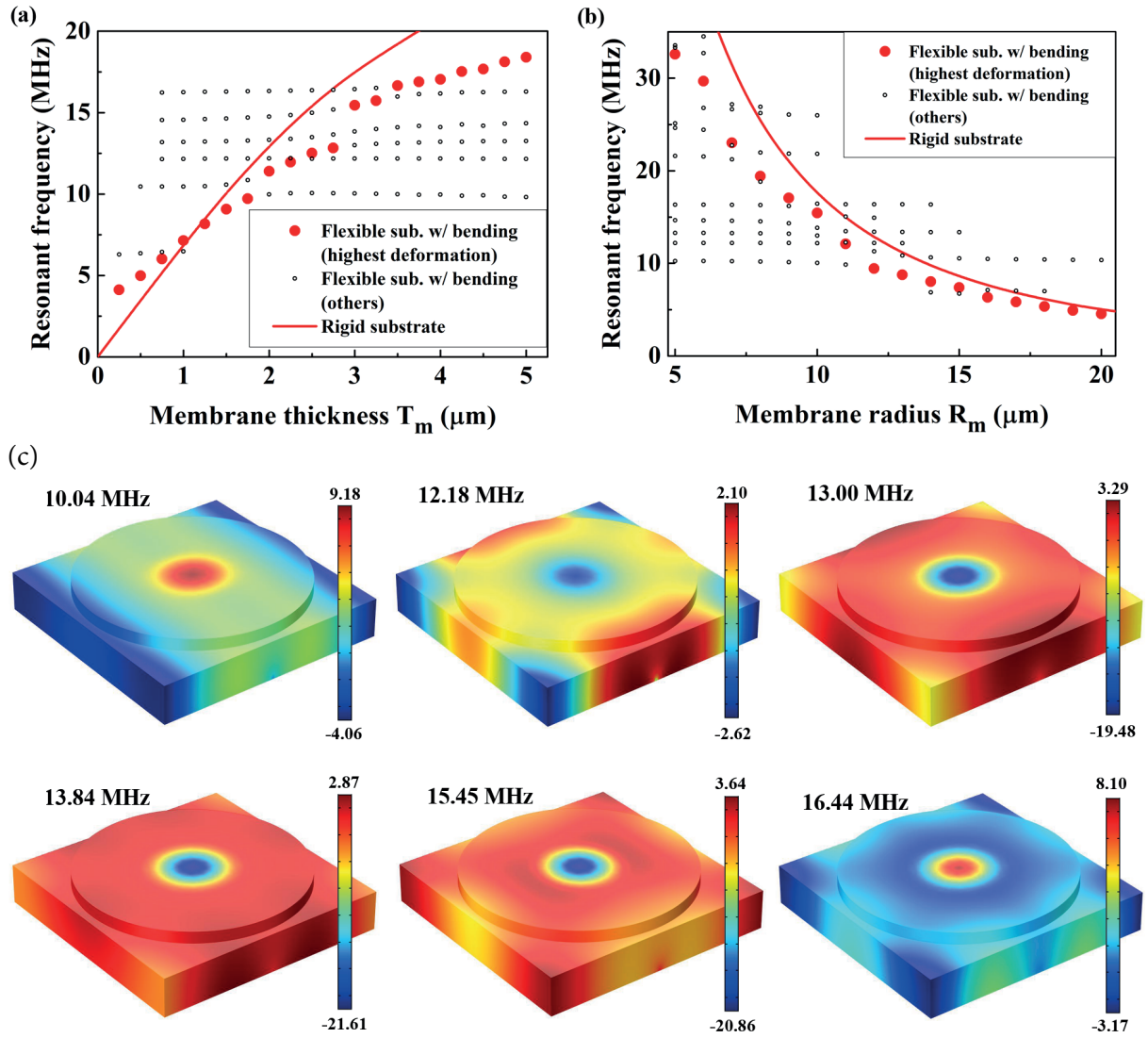

Figure 7. (a, b) Calculated resonant frequencies as a function of (a) membrane thickness T_m and (b) membrane radius R_m. Solid line: on a rigid substrate and without bending. Symbols: on a flexible substrate and with bending (radius: 1 mm); only the resonant frequencies whose mode profiles are that of fundamental ones in the membrane are plotted; closed circles (red) indicate the ones with highest deformation magnitude for that geometry. For nonvarying geometries, nominal values (Table) are used, except in (b) where W_{an} is changed as well to keep $R_m + W_{an}$ constant as 28 μm. (c) Deformation profiles of a full device with the nominal geometry at various resonant frequencies. For a device with the nominal geometry, 15.45 MHz exhibits the highest magnitude of deformation. Color legend: relative deformation magnitude (arbitrary unit).

with fundamental mode profiles in the membrane. It can be seen that different mode profiles are found in the substrate as well as in the anchor part. Among the six resonant frequencies presented, 15.45 MHz exhibits the highest magnitude of deformation. These resonant frequencies with highest magnitudes of deformation are indicated in Figures 7a and 7b as closed circles in red. It can be also seen from Figures 7a and 7b that the values of the resonant frequencies that are not associated with the highest deformation remain relatively constant, without being much affected by the device geometries.

One can see that the resonant frequencies with highest deformation roughly follow the trend of those from a membrane on a rigid substrate. For a membrane thicker than 1 μm, the resonant frequencies of the ones on a flexible substrate after bending are lower than those of the ones on a rigid substrate. This is because the membrane is anchored to a flexible substrate so that the effective spring constant is reduced. However, for a membrane thinner than 1 μm, the resonant frequencies of the ones on a flexible substrate after bending are higher than those of the ones on a rigid substrate. This is due to increased membrane stiffness caused by tensile stress induced by bending. Such a stiffening has a stronger effect on a thinner membrane. In the case of a thicker membrane, that stiffening effect is overshadowed by the effect of a soft anchor. A similar trend is seen from Figure 7b, i.e. as the membrane radius increases, its stiffness decreases so that the soft-anchor effect is caught up by the stress-induced stiffening effect.

Overall, the relationship between the membrane radius and the resonant frequency is as expected, i.e. increase in the mass and decrease in stiffness both work in the direction of a lower resonant frequency. The relationship between the membrane thickness and the resonant frequency is also as expected, i.e. increase in the stiffness by increased thickness outweighs that in mass to result in increased resonant frequency. Other device geometries do not affect the resonant frequency significantly. It is also learned that in order to meet the design goal of 20 MHz resonant frequency, the membrane radius has to be smaller than 7.7 μm for the thickness of 3 μm, which is achievable in practice.

3.4. Pull-in voltage

Pull-in voltage is another important design parameter of a CMUT device as the DC bias to the transducer is typically set as 80%–90% of the pull-in voltage. Figure 8 shows the effect of device geometries to the pull-in voltage for two different cases: (1) on a flexible substrate with bending, and (2) on a rigid substrate without bending. The relationships between the design parameters and the pull-in voltages are as expected: the pull-in voltage increases as (a) membrane thickness T_m increases, (b) membrane radius R_m decreases, (c) dielectric layer thickness T_{di} increases, and (d) air gap thickness d_{air} increases. For almost all design parameters, the pull-in voltages in the case of a flexible substrate with bending were lower than those of a rigid substrate without bending. This is mainly due to the closing of the gap between the membrane and the dielectric layer, as shown in Figure 4d. There is another effect of bending, which works in the opposite direction. The tensile stress induced by bending increases the spring constant and therefore increases the pull-in voltage. However, in almost all cases of design consideration, the effect of reduced air gap was more dominant than that of the tensile stress so that the pull-in voltage was lowered, as presented in Figure 8. Nevertheless, the effect of the tensile stress can be seen with the very thin membrane cases (<1 μm). For example with T_m of 0.2 μm, the pull-in voltage is higher in the case of a flexible substrate with bending even though the center gap reduction (18.3 nm) is similar to the case where T_m is 1 μm (center gap reduction: 21.8 nm). This is because the induced stress affects the spring constant more heavily in the case of a thinner membrane than it does for a thicker membrane. This finding is in accordance with the one obtained in regards to the resonant frequency as discussed in Section 3.3. Effects of other parameters (W_{an}, T_s, and T_{be}) on the pull-in voltage were negligible as expected.

The main drawback of typical polymer materials is the low breakdown field (dielectric strength). For example, the dielectric strength of PMMA is 20$\pm$2 MV/m, which means that the maximum voltage a PMMA layer of 250 nm thickness can take is 5$\pm$0.5 V. One can increase this voltage by making the dielectric layer thicker. However, this also increases the pull-in voltage, which cancels out such an advantage. Alternatively, one can reduce the membrane thickness or increase the membrane radius to reduce the pull-in voltage, as can be

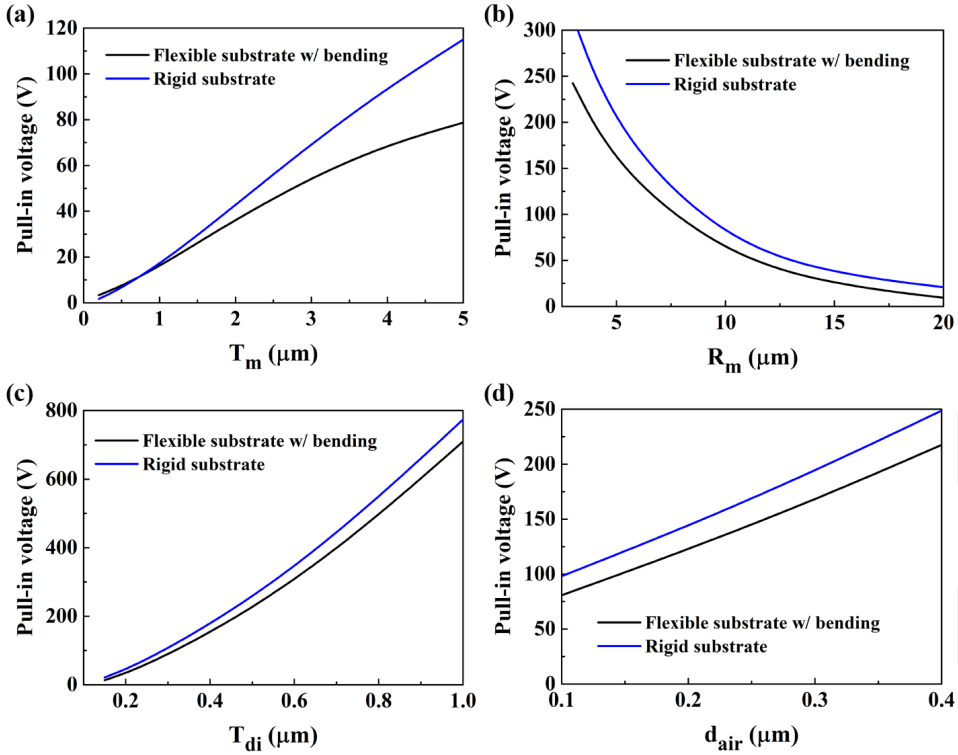

Figure 8. Calculated pull-in voltage as a function of (a) membrane thickness T_m, (b) membrane radius R_m, (c) dielectric thickness T_{di}, and (d) air gap thickness d_{air}, for two different conditions: (black) flexible substrate and with bending (radius: 1 mm), and (blue) rigid substrate and without bending. For nonvarying geometries, nominal values (Table) are used, except for the following cases: in (b) W_{an} is changed as well to keep R_m + W_{an} constant as 28 μm; in (c) d_{air} is set to be T_{di} - 0.1 μm; in (d) T_{di} is 0.5 μm.

deducted from Figure 8. However, it reduces the resonant frequency significantly. This is the major limitation of the all-polymer CMUTs. One should either operate the device at a very low DC bias with lower coupling efficiency or develop a new polymer material that has higher dielectric strength.

3.5. Conclusion

In this work, an all-polymer CMUT array was studied for an IVUS application. The transducer array is to be wrapped around a cylindrical frame so that a cross-section view of blood vessels can be obtained without the need for mechanical rotation rendered externally. FEA was used to study the effects of substrate bending and different geometries on the characteristics of the CMUTs. It was found that the mechanical resonant frequency of the transducer membrane was decreased because of a soft anchor when it was fabricated on a flexible substrate. On the other hand, tensile stress induced by substrate bending had an effect of increasing the resonant frequency. A condition was established for the transducer membrane geometries to achieve a design target of 20 MHz of resonant frequency: radius = 7.7 μm, thickness = 3 μm for a PEDOT:PSS membrane. Substrate bending showed two counteracting effects on the pull-in voltage: reduction in the air gap that decreases it and tensile stress induced that increases it. In almost all device geometries, the pull-in voltage was higher than the magnitude that a PMMA dielectric layer can endure. It was concluded that either the all-polymer CMUTs have to be operated at a very low DC bias or a new polymer material with higher dielectric strength has to be developed for this application.

Acknowledgment

This work was partially supported by the Research Fund of Abdullah Gül University (Project Number: FOA-2016-49).

References

[1] Born N, Lancee CT, Van Egmond FC. An ultrasonic intracardiac scanner. Ultrasonics 1972; 10: 72-76.

[2] Carlier SG, Tanaka K. Studying coronary plaque regression with IVUS: a critical review of recent studies. J Interv Cardiol 2006; 19: 11-15.

[3] Logani S, Saltzman HE, Kurnik P, Eisen HJ, Ledley GS. Clinical utility of intravascular ultrasound in the assessment of coronary allograft vasculopathy: a review. J Interv Cardiol 2011; 24: 9-14.

[4] Zhang YJ, Pang S, Chen XY, Bourantas CV, Pan DR, Dong SJ, Wu W, Ren XM, Zhu H, Shi SY et al. Comparison of intravascular ultrasound guided versus angiography guided drug eluting stent implantation: a systematic review and meta-analysis. BMC Cardiovasc Disor 2015; 15: 153.

[5] Mintz GS, Nissen SE, Anderson WD, Bailey SR, Erbel R, Fitzgerald PJ, Pinto FJ, Rosenfield K, Siegel RJ, Tuzcu EM et al. American College of Cardiology clinical expert consensus document on standards for acquisition, measurement and reporting of intravascular ultrasound studies (ivus). J Am Coll Cardiol 2001; 37: 1478-1492.

[6] Chang M, Deng HC, Pang DC, Chen MY. A novel method for fabricating sonic paper. In: IEEE International Ultra Symposium; New York, NY, USA; 2007. pp. 527-530.

[7] Kim S, Zhang X, Daugherty R, Lee E, Kunnen G, Allee DR, Forsythe E, Chae J. Microelectromechanical systems (MEMS) based-ultrasonic electrostatic actuators on a flexible substrate. IEEE Electr Device L 2012; 33: 1072-1074.

[8] Caliano G, Caronti A, Savoia A, Longo C, Pappalardo M, Cianci E, Foglietti V. Capacitive micromachined ultrasonic transducer (cMUT) made by a novel reverse fabrication process. In: IEEE International Ultra Symposium; Rotterdam, the Netherlands; 2005. pp. 479-482.

[9] Caroni A, Coppa A, Savoia A, Longo C, Gatta P, Mauti B, Corbo A, Calabrese B, Bollino G, Paz A et al. Curvilinear capacitive micromachined ultrasonic transducer (CMUT) array fabricated using a reverse process. In: IEEE International Ultra Symposium; Beijing, China; 2008. pp. 2092-2095.

[10] Dickinson RJ, Kitney RI. Miniature ultrasonic probe construction for minimal access surgery. Phys Med Biol 2004; 49: 3527-3538.

[11] Zhuang X, Lin DS, Oralkan O, Khuri-Yakub BT. Fabrication of flexible transducer arrays with through-wafer electrical interconnects based on trench refilling with PDMS. J Microelectromech S 2008; 17: 446-452.

[12] Cheng X, Chen J, Shen IM, Li PC, Wang M. Fabrication and assembly of a monolithic 3D CMUT array for imaging applications. In: IEEE International Ultra Symposium; New York, NY, USA; 2007. pp. 515-518.

[13] Hah D, Je CH, Lee SQ. Design of capacitive micromachined ultrasonic transducers (CMUTs) on a flexible substrate for intravascular ultrasonography (IVUS) applications. In: Symposium on Design, Test, Integration and Packaging of MEMS/MOEMS; Bordeaux, France; 2017. pp. 167-171.

[14] Ladabaum I, Jin X, Soh HT, Atalar A, Khuri-Yakub BT. Surface micromachined capacitive ultrasonic transducers. IEEE T Ultrason Ferr 1998; 45: 678-690.

[15] Yaralioglu GG, Ergun AS, Bayram B, Hæggstrom E, Khuri-Yakub BT. Calculation and measurement of electromechanical coupling coefficient of capacitive micromachined ultrasonic transducers. IEEE T Ultrason Ferr 2003; 50: 449-456.

[16] Mahmud MM, Adelegan OJ, Sanders JL, Zhang X, Yamaner FY, Dayton PA, Oralkan O. Improved CMUT structure and method of operation for dual-frequency acoustic angiography. In: IEEE International Ultra Symposium; Washington, DC, USA; 2017.

[17] Belgacem B, Calame F, Muralt P. Design, modeling and fabrication of piezoelectric micromachined ultrasonic transducers. In: IEEE International Ultra Symposium; Rotterdam, the Netherlands; 2005. pp. 483-486.

[18] Wang T, Lee C. Zero-bending piezoelectric micromachined ultrasonic transducer (pMUT) with enhanced transmitting performance. J Microelectromech S 2015; 24: 2083-2091.

[19] Younis MI, Nayfeh AH. A study of the nonlinear response of a resonant microbeam to an electric actuation. Nonlinear Dynam 2003; 31: 91-117.